Supporting Information

Dual-Use Synthesis of an Asymmetric Anthraquinone Heptyl Viologen (AQHV) for Solution and Gel-Polymer Electrolyte-based Electrochromic Device

Rambabu Sydam,[†] Gaurav Kumar Silori,[†]Hui-Chieh Hsu [†] Kuo-Chuan Ho [†,‡,§]*

[†] Department of Chemical Engineering, National Taiwan University, Taipei 10617, Taiwan

[‡] Institute of Polymer Science and Engineering, National Taiwan University, Taipei 10617, Taiwan

[§] Advanced Research Center of Green Materials Science and Technology, National Taiwan University, Taipei 10617, Taiwan

[*]Corresponding author: Tel.: +886–2–2366–0739; Fax: +886–2–2362–3040

E–mail: kcho@ntu.edu.tw

S1: Discussions

S1.1: Radical formation in $AQHV^{2+}$

Formation of π-dimers for individual viologen radical cations or anthraquinone radical anions of $AQHV^{2+}$:

$$2\ AQHV^{+\bullet} \leftrightarrow (AQHV)_2^{2+} \quad \text{or} \quad \pi\text{-}(HV^{+\bullet} - HV^{+\bullet}), \tag{S1}$$

$$2\ AQ^{-\bullet}HV^{2+} \leftrightarrow (AQHV)_2^{2+} \quad \text{or} \quad \pi\text{-}(AQ^{-\bullet} - AQ^{-\bullet}). \tag{S2}$$

S1.2: Cyclic Voltammetry (CV) and Differential Pulse Voltammetry (DPV) Studies:

The **Figure S8a** shows the CV of $AQHV(BF_4)_2$ in a limited potential window (–0.9 V to +0.2 V), where only the first reversible redox couple is observed. This corresponds to the one-electron reduction of the viologen core ($AQHV^{2+}/AQHV^{+\bullet}$) and its oxidation back, with cathodic and anodic peak potentials at approximately –0.78 to –0.81 V and –0.65 to –0.68 V, respectively. **Figure S8b** shows the CV in an extended window (–1.0 V to +0.2 V), revealing both a fully reversible and the beginning of a second redox couple formation (around -0.95 V to -1.0 V). **Figure S8c**, recorded in the full potential window (-1.5 V to +0.2 V), shows two well-defined redox events. The first redox couple appears at E_{pc1} (-0.78 V) and E_{pa1} (–0.66 V) (consistent with the viologen first one-electron reduction and its re-oxidation process), while the second broader redox event occurs around E_{pc2} (–1.28 V) and E_{pa2} (–1.05 V), which we attribute to the reduction involving the AQ moiety. This assignment is favoured over the alternative possibility of a second one-electron reduction of the viologen radical cation, which would instead yield di-reduced viologen unit $AQHV^{(0)}$. These stepwise reductions are attributed to sequential one-electron processes, likely corresponding to $AQHV^{2+}/AQHV^{+\bullet}$ (first reduction) and either $AQHV^{+\bullet}/AQHV^{(0)}$ or $AQHV^{+\bullet}/AQ^{-\bullet}HV^{+\bullet}$ (second reduction), depending on the

influence of the anthraquinone (AQ) moiety in AQHV. If such a di-reductions ($AQHV^{+\bullet}/AQHV^{(0)}$) were dominant, the electrochromic device would be expected to exhibit a bleached (colourless) state. However, as shown in **Figure 4d**, the device remains in a stable blue-colored state even beyond –1.2 V, supporting the formation of a zwitterionic radical species ($AQ^{-\bullet}HV^{+\bullet}$) instead. This confirms the first and second one-electron reduction steps yield zwitterionic radical species ($AQ^{-\bullet}HV^{+\bullet}$). These observations confirm that the redox processes occur stepwise via two sequential one-electron transfers: first the $AQHV^{2+}/AQHV^{+\bullet}$ couple, followed by a second reduction, most plausibly $AQHV^{+\bullet}/AQ^{-\bullet}HV^{+\bullet}$. The influence of the AQ moiety plays a crucial role in stabilizing this zwitterionic radical, as further supported by the DPV results in the following section (**Figures S10 and S11**), which reveal overlapping reduction features and enhanced current response indicative of both redox-active sites contributing.

To further clarify the species involved in these redox processes, we performed DPV measurements, which help resolve overlapping redox events. The observed shifts in peak positions and the increased current intensity in the DPV of $AQ^{-\bullet}HV^{+\bullet}$ (compared to $AQHV^{+\bullet}$ alone) support the formation of a new redox-active species. The broader CV features and increased redox current densities suggest enhanced redox activity, which is consistent with the presence of a zwitterionic radical species. Collectively, these new electrochemical data support our claim that stepwise one-electron reductions of the AQ and HV units lead to the formation of a zwitterionic radical ($AQ^{-\bullet}HV^{+\bullet}$). This species likely facilitates enhanced electron transfer properties and contributes to the improved performance observed in our electrochromic device studies. To further support the formation of zwitterionic radical species in $AQHV(BF_4)_2$, we performed comparative CV and DPV analyses of the individual components $HV(BF_4)_2$ and AQ (2-bromomethyl anthraquinone), alongside the AQHV salt, within an extended potential window (–1.6 V to +0.2 V). These measurements provide critical insight into the stepwise redox events and the possible formation of $AQ^{-\bullet}HV^{+\bullet}$ species. The CV of $HV(BF_4)_2$

(**Figure S9b**) reveals two distinct and reversible redox couples centered at –1.25/–1.20 V and -1.35/-1.28 V. These correspond to the two sequential one-electron reductions of the viologen core, forming first $HV^{+\bullet}$ and then the neutral $HV^{(0)}$ species. The CV of AQ under the same conditions (**Figure S9c**) shows redox events at –1.20/–1.15 V and –1.55/–1.50 V, corresponding to the well-known two-step, one-electron reduction of the anthraquinone core. Notably, the second reduction (at more negative potentials) indicates that the peak may be less well-defined and potentially broader than in a reversible system, both anodic and cathodic peaks are still observed. In contrast, the CV of $AQHV(BF_4)_2$ (**Figure S9a**) reveals: (i) a first reversible redox couple at –0.80/–0.75 V, attributed to the reduction of the viologen core ($AQHV^{2+} \rightarrow AQHV^{+\bullet}$) and (ii) a broad, composite second redox region spanning –1.1 V to –1.4 V with peaks centered around –1.25/–1.20 V. This potential range overlaps with both the $AQ^{-\bullet}$ formation and the second reduction of $HV^{+\bullet}$ to $HV^{(0)}$. This overlapping region suggests a competitive interaction between the AQ moiety and the viologen radical cation ($HV^{+\bullet}$) for the second electron. The potential alignment and broadening in this region indicate that the second one-electron reduction of $AQHV^{+\bullet}$ may not proceed via a simple $AQHV^{+\bullet}$ to $AQHV^{(0)}$ pathway. Instead, the data support an intermediate stage where a zwitterionic radical species ($AQ^{-\bullet}HV^{+\bullet}$) forms due to the simultaneous presence of a radical anion on the AQ unit and a radical cation on the HV unit.

However, we acknowledge that CV alone cannot unambiguously prove the zwitterionic radical configuration. To further elucidate the nature of the overlapping redox processes, we carried out DPV analysis **(Figure S10a**). The DPV provides better peak resolution, revealing multiple closely spaced reduction events in the –1.1 V to –1.4 V range. These peaks are consistent with: (a) The reduction of AQ moiety in $AQHV^{+\bullet}$ to form $AQ^{-\bullet}HV^{+\bullet}$, followed by (b) A third one-electron reduction, converting $AQ^{-\bullet}HV^{+\bullet}$ to $AQ^{-\bullet}HV^{(0)}$. Together, these results strongly support the sequential formation of a zwitterionic radical intermediate ($AQ^{-\bullet}HV^{+\bullet}$), followed by further reduction. This interpretation is consistent with the potential shifts observed and the competition between redox-active centers within

the asymmetric AQHV structure. To account for the overlapping region observed in the CV (**Figure S9a**), we conducted detailed DPV studies of $AQHV(BF_4)_2$ and compared the results with those of the individual $HV(BF_4)_2$ and AQ moieties under identical conditions. These DPV measurements provide deeper insights into the multi-electron transfer processes and the possible formation of zwitterionic radical intermediates. As shown in **Figure S10a**, the DPV curve of $AQHV(BF_4)_2$ at a standard scan rate of 5 mV/s reveals multiple distinct reduction peaks. Notably, two overlapping peaks appear around -1.2 V vs. Ag/Ag^+, indicating closely spaced redox events likely associated with successive one-electron reductions of the $AQHV^{+\bullet}$ species. To improve resolution of these events, we performed DPV at a slower scan rate of 0.75 mV/s. The resulting data (**Figure S10b**) reveal four distinct reduction peaks at approximately -0.76 V (peak 1), -1.14 V (peak 2), -1.25 V (peak 3), and -1.50 V (peak 4). **Peak 1** corresponds to the first one-electron reduction of $AQHV^{2+}$ to $AQHV^{+\bullet}$ (i.e., viologen-centered reduction). **Peaks 2 and 3** fall within the range of the known first reduction of the AQ moiety and the second reduction of the viologen core, respectively (supported by CV data in **Figures S9b and S9c**). **Peak 4** around –1.50 V aligns with the second one-electron reduction of the AQ unit ($AQ^{-\bullet} \rightarrow AQ^{2-}$), completing the four-step process. The resolution of peaks 2 and 3 provides critical evidence that these two redox events occur in close proximity, supporting our proposal of the formation of a zwitterionic radical species ($AQ^{-\bullet}HV^{+\bullet}$). Specifically, peak 2 is attributed to the first one-electron reduction of the AQ moiety within $AQHV^{+\bullet}$, while peak 3 corresponds to the second one-electron reduction of the viologen center ($AQHV^{+\bullet}$). Their near-overlapping potentials and the relative current intensities suggest a competitive yet sequential process that stabilizes the intermediate $AQ^{-\bullet}HV^{+\bullet}$ species, i.e., a zwitterionic radical. These observations now provide scientific validation for the formation of zwitterionic radicals upon two-electron reduction of $AQHV^{2+}$ and align with the presented **Scheme 3 (Equation 2)** in the manuscript. Furthermore, the close spacing of these redox events highlights the importance of scan rate optimization in differentiating closely coupled multi-electron transfer processes. In conclusion, the combined CV and DPV analyses clearly support the stepwise electron

transfer pathway leading to the formation of $AQ^{-\bullet}HV^{+\bullet}$ and stability of the zwitterionic radical intermediates in the AQHV system.

Moreover, the CV and DPV data of $HV(BF_4)_2$, presented in the **Figure S10c and d**, provide important insights into its redox behaviour. The CV reveals two distinct redox couples centered around –0.80 V and –1.30 V vs. Ag/Ag^+ (**Figure S10c**), corresponding to the sequential one-electron reductions of the viologen core: The first redox couple (E_pc_1 at –0.84 V, E_{pa1} at –0.76 V) is attributed to the reduction of HV^{2+} to the radical cation $HV^{+\bullet}$. The second couple (E_pc_2 at -1.34 V, E_{pa2} at -1.27 V) corresponds to the further reduction of $HV^{+\bullet}$ to the neutral $HV^{(0)}$ state. These assignments are supported by DPV measurements, which show two well-defined peaks at approximately -0.82 V and -1.32 V. The first peak corresponds to the $HV^{2+}/HV^{+\bullet}$ transition, while the second indicates complete reduction to the neutral form $HV^{(0)}$ ($HV^{+\bullet}/HV^{(0)}$). Extension of the potential window to -1.5 V confirms access to the full two-electron reduction process, indicating that $HV(BF_4)_2$ can be fully reduced under the studied conditions. Together, these results validate the reversible two-step redox behaviour of the viologen moiety and establish a baseline for comparison with the more complex redox processes observed in the asymmetric $AQHV(BF_4)_2$, where electronic interactions between the AQ and HV units influence redox potentials and intermediate species formation. Besides, the DPV of 2-bromomethyl anthraquinone (AQ) in the electrolyte reveals two primary reduction peaks with half-wave potentials at approximately -1.25 V and -1.85 V (**Figure S11d**), corresponding to two distinct one-electron reductions. Complementarily, the CV profile of AQ (**Figure S11a**) exhibits two reduction peaks at -1.23 V and -1.55 V, which is characteristic of anthraquinone (AQ) undergoing sequential one-electron reduction processes. However, when incorporated into the $AQHV(BF_4)_2$ structure, the electrochemical behaviour of the AQ moiety may be significantly influenced by the presence of the viologen (HV) unit. To elucidate these effects, we have compared the CV responses of $AQHV(BF_4)_2$ with those of the individual AQ and $HV(BF_4)_2$ species. These comparisons provide important insights into the redox

behaviour of the individual components, as well as how their electronic interactions modulate the redox properties when they are integrated into a single asymmetric molecular species.

S1.3: Electron Paramagnetic Resonance (EPR) Studies:

The electrochemical cell consisted of a three-electrode configuration embedded within a flat quartz EPR tube (EPR Model: Bruker EMX-plus). A platinum wire served as the working electrode, with additional platinum wires functioning as the counter and quesi-reference electrodes. All potentials are reported with respect to the Pt wire reference. The electrolyte solution was composed of 10 mM AQHV and 0.1 M tetra-n-butylammonium tetrafluoroborate ($TBABF_4$) dissolved in propylene carbonate (PC). The EPR cell was filled with this solution under ambient conditions. Electrochemical control was achieved using a potentiostat, and spectra were recorded at various applied potentials to monitor the formation of paramagnetic species. All spectra were recorded at room temperature with a microwave power of 1 mW. Signal intensity and spectral features were analysed to confirm the presence and evolution of radical species upon electrochemical reduction of $AQHV^{2+}$, HV2+, and AQ (2-bromomethyl anthraquinone).

The *in-situ* EPR analysis reveals that AQHV begins forming paramagnetic species at -0.5 V, with a clear and stable radical signal observed from -0.7 V to -1.2 V (**Figure S14)**. The g-factor remains around 2.0037 throughout this range, characteristic of stable organic radicals. [1–4] At more negative potentials, particularly -1.5 V and -1.8 V, additional splitting appears in the spectra, suggesting further redox processes. The behaviour of $HV(BF_4)_2$ closely mirrors that of $AQHV^{2+}$, showing the onset of EPR activity at -0.5 V and a strong, stable signal in the same potential window. The g-factor for HV salt at -0.9 V (2.00406) closely matches that of $AQHV^{+\bullet}$ derived derivative, confirming the generation of the $HV^{+\bullet}$ radical in the $HV(BF_4)_2$.[2,3] On the other hand, AQ alone does not display any EPR signal across the studied potential range, consistent with its known electrochemical behaviour involving a rapid two-electron reduction behaviour.[1] Since, the CV profile of AQ shows two closely spaced

cathodic peaks (E_{pc1} = –1.23 V and E_{pc2} = –1.50 V), indicative of a direct two-electron transfer from AQ to AQ^{2-}. This process bypasses the radical intermediate ($AQ^{-\bullet}$), hence no detectable EPR signal.[1] While the EPR signal is dominated by features consistent with $HV^{+\bullet}$, the possibility of $AQ^{-\bullet}$ contributions—especially at more negative potentials cannot be ruled out. However, no direct EPR evidence of $AQ^{-\bullet}$ was observed in the isolated AQ system, suggesting that the zwitterionic radical $AQ^{-\bullet}HV^{+\bullet}$ is only stabilized within the hybrid structure of $AQHV^{2+}$.[3,4]

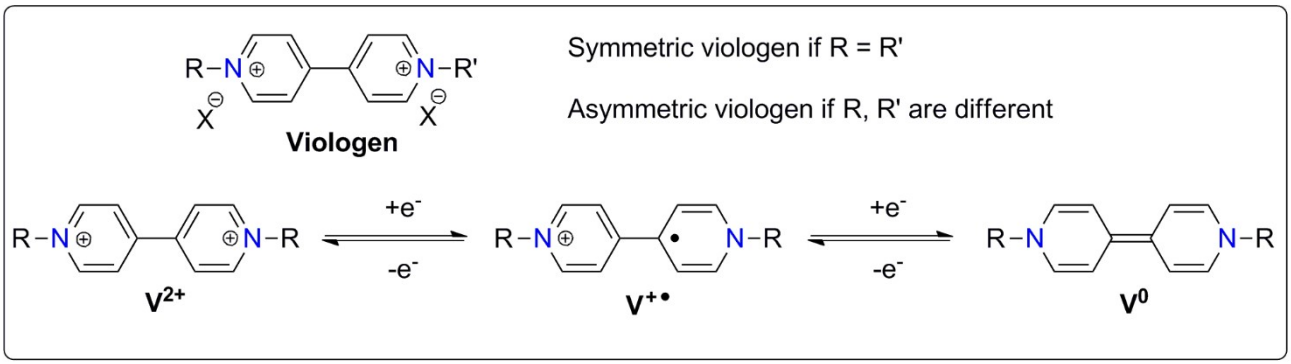

Scheme S1. The three common redox forms of viologen.

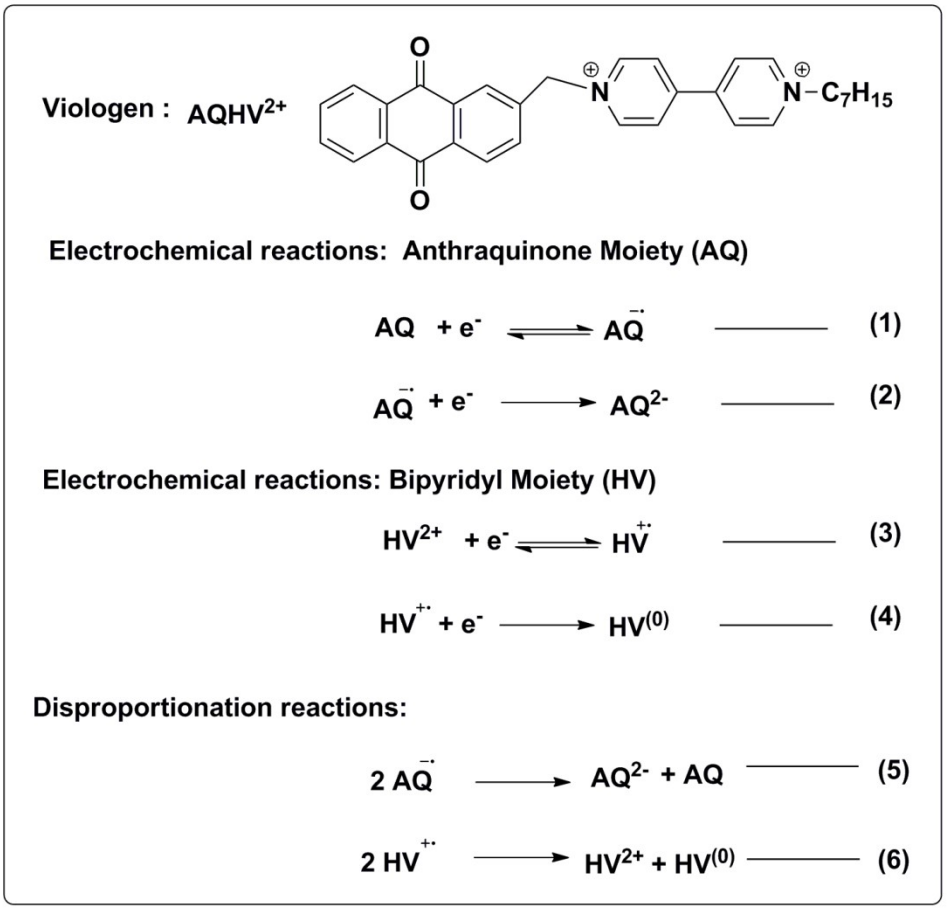

Scheme S2. At the top: Structure of anthraquinone heptyl viologen (dication). Next: Formation of different species in the ECD, containing AQHV and Fc, under high applied potentials greater than 1.0 V.

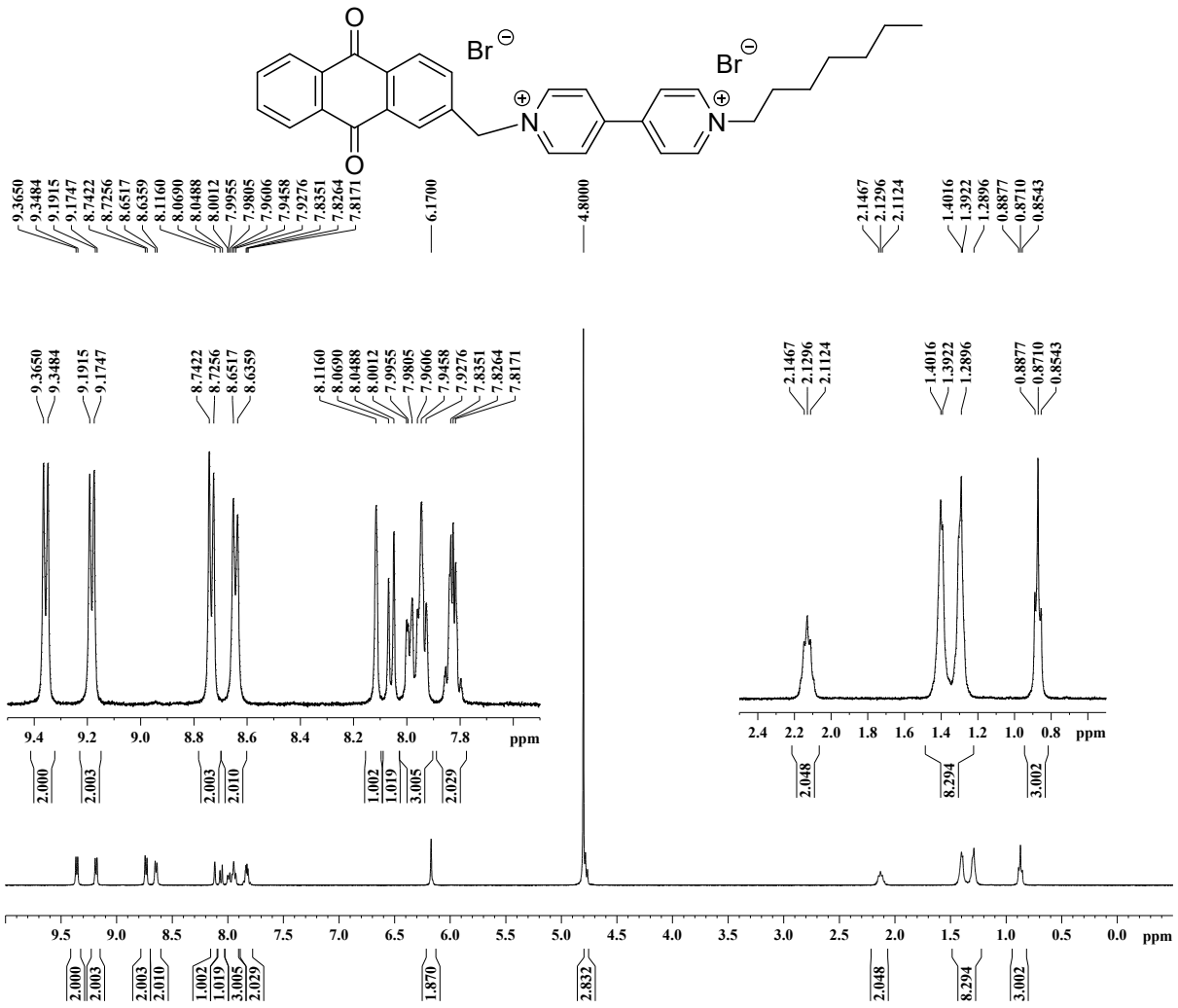

Figure S1. ^{1}H NMR (500 MHz) spectrum of $AQHVBr_2$ in D_2O.

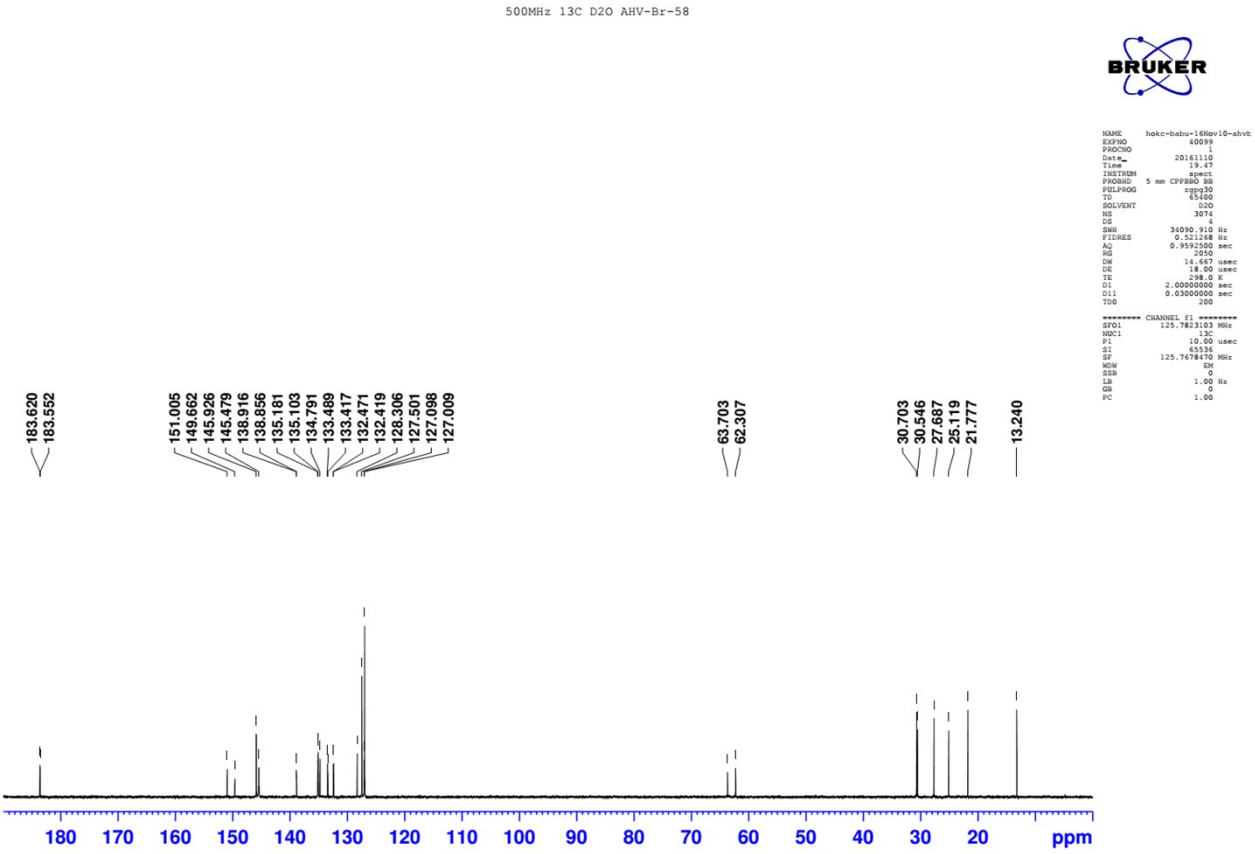

Figure S2. ^{13}C NMR (100 MHz) spectrum of AQHVBr$_2$ in D_2O.

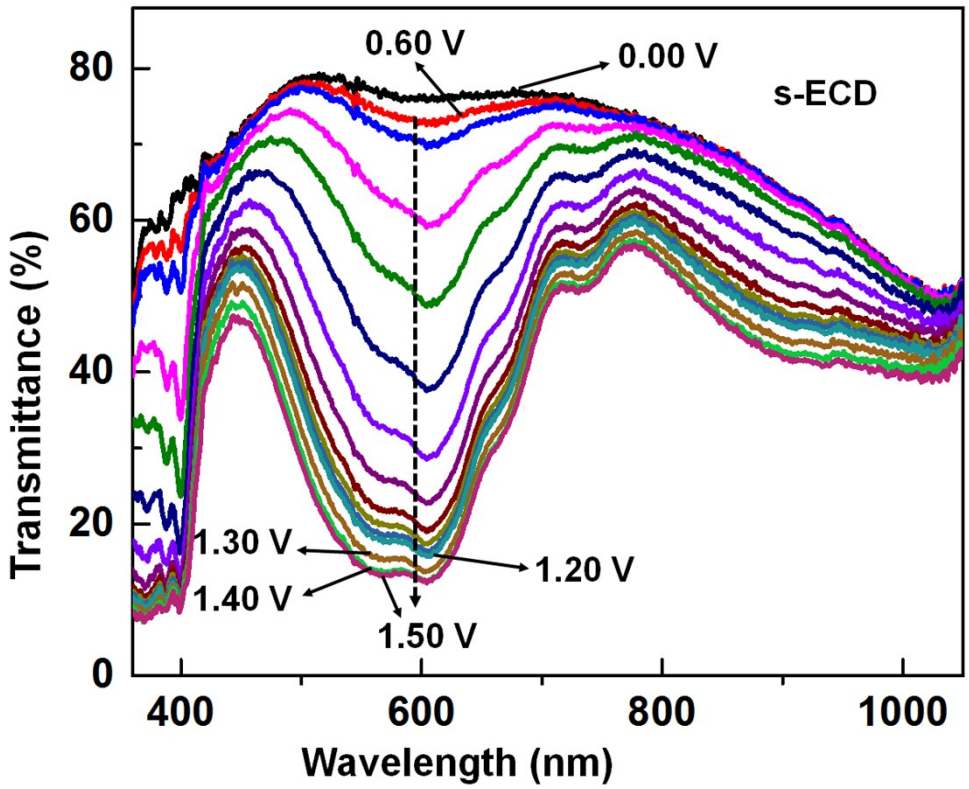

Figure S3. *In-situ* UV−visible transmittance spectra of the s-ECD with AQHV–Fc, recorded under different potentials of 0.60 V to 1.20 V, in steps of 0.05 V, and also at 1.30. 1.40, 1.50 V and 0.00 V.

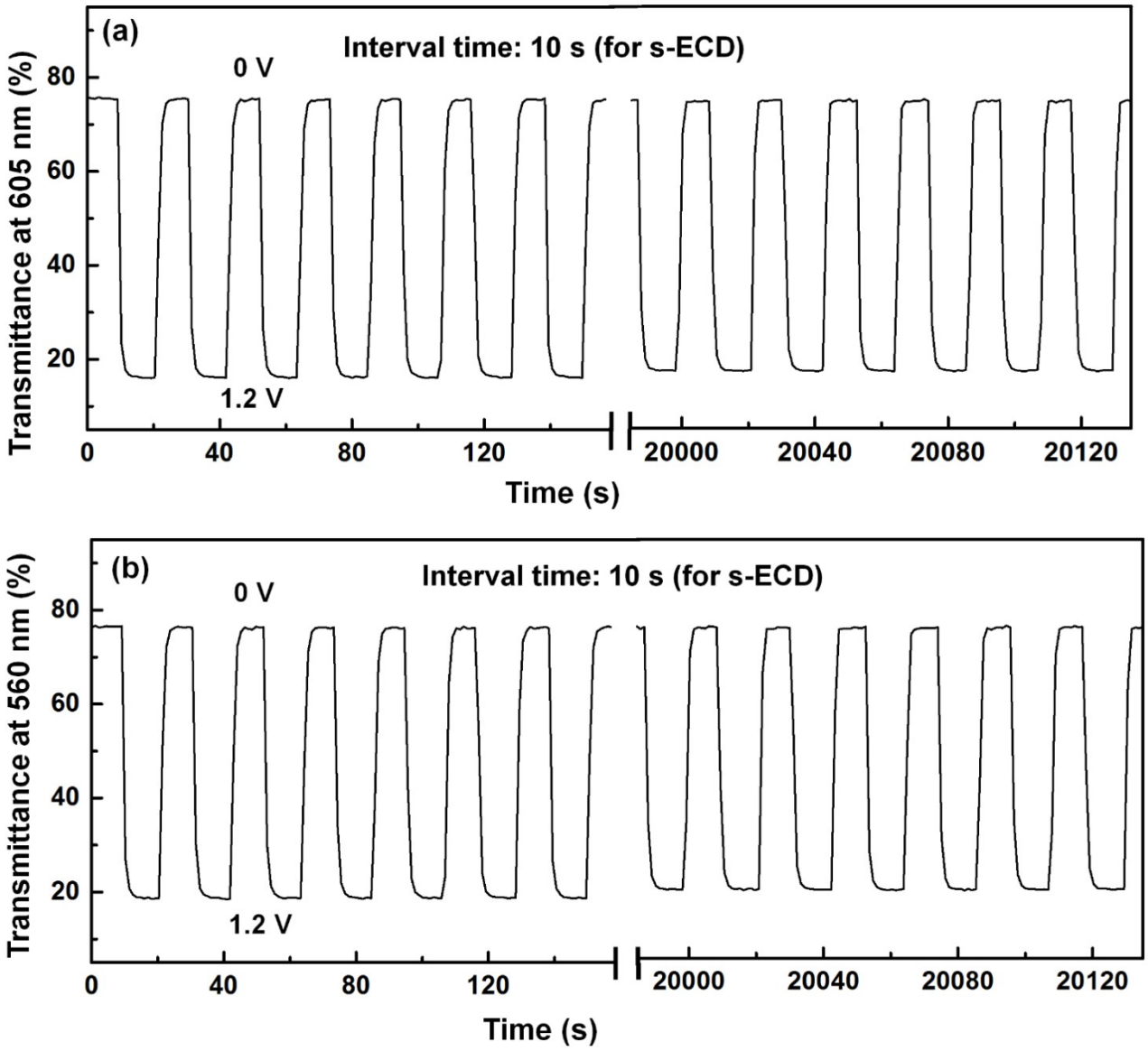

Figure S4. Dynamic transmittance responses of the s-ECD after 1000th cycles, at the wavelengths of (a) 605 nm (λ_{max}) and (b) 560 nm, under continuous cycling between 0.0 and 1.2 V, at the same step time of 10 s.

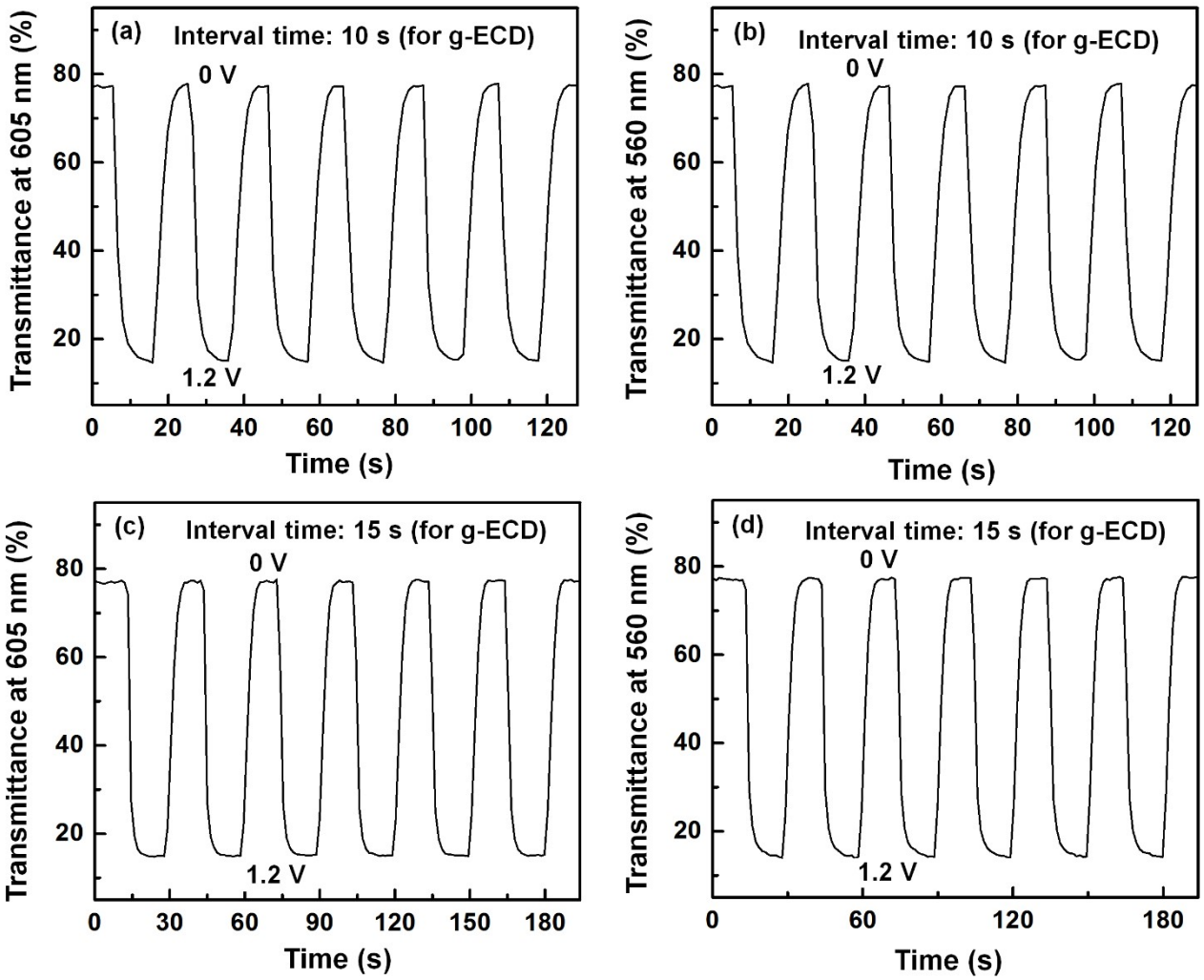

Figure S5. (a) Dynamic transmittance curves of the g-ECD for an interval time of 10 s obtained at 605 nm, (b) the curves of g-ECD for an interval time of 10 s obtained at 560 nm, (b) the curves of g-ECD for an interval time of 15 s obtained at 605 nm, and (d) the curves of g-ECD for the interval time of 15 s obtained at 560 nm. All the curves were obtained under continuous cycling between 0.0 and 1.2 V.

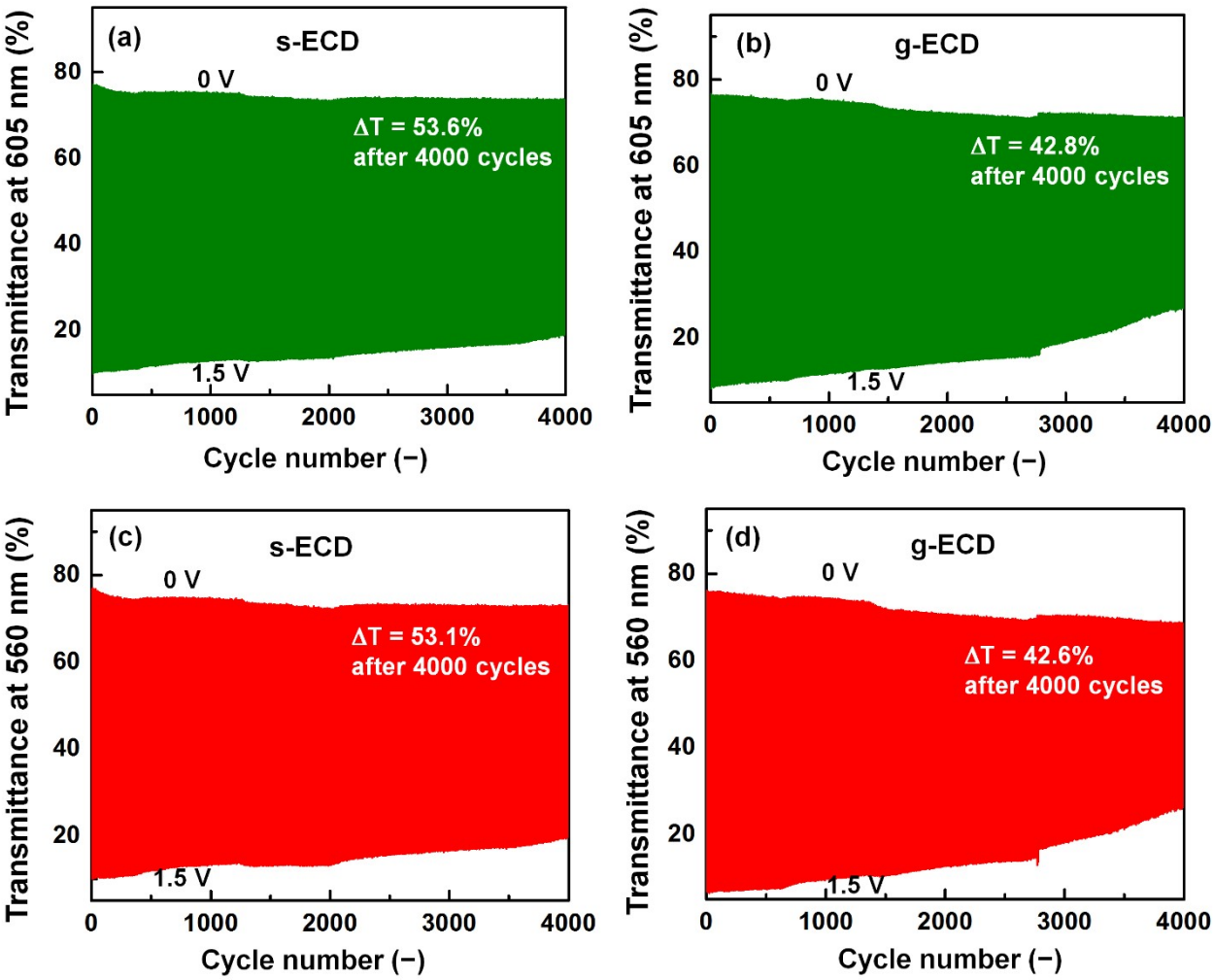

Figure S6. (a) Transmittance of s-ECD at its first cycle and 4000th cycle at 605 nm, (b) transmittance of the g-ECD at its first cycle and 4000th at 605 nm, (c) transmittance of the s-ECD at its first cycle and 4000th cycle at 560 nm, and (d) transmittance of the g-ECD at its first cycle and 4000th cycle at 560 nm; in all the cases the transmittances were obtained under continuous cycling between 0.0 V and 1.5 V, and the interval times are 10 s and 15 s for s-ECD and g-ECD, respectively.

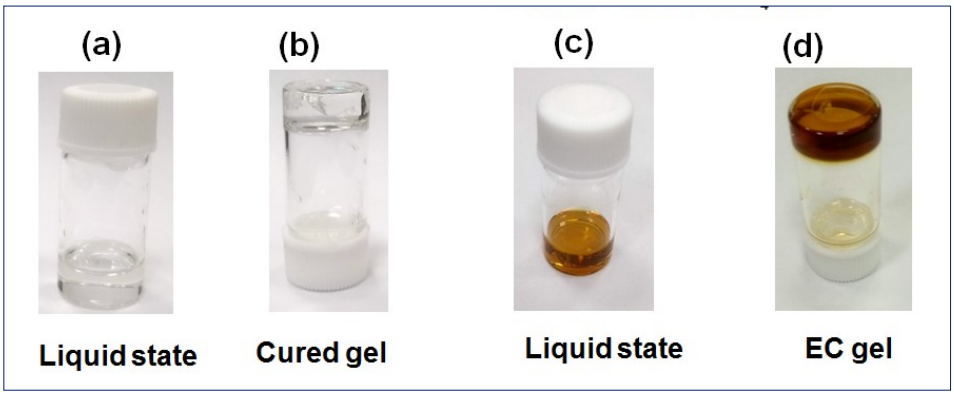

Figure S7. Photographs of (a) liquid state gel precursor solution containing $TBABF_4$ (0.5 M), 20% MMA and 5% EGDMA based on MMA in PC, (b) its cured polymeric gel electrolyte, (c) the EC gel precursor solution containing $AQHV(BF_4)_2$ (50 mM), ferrocene (Fc, 50 mM) and $TBABF_4$ (0.5 M) in the liquid state gel precursor as mentioned in (a), and (d) cured EC polymeric gel electrolyte of (c).

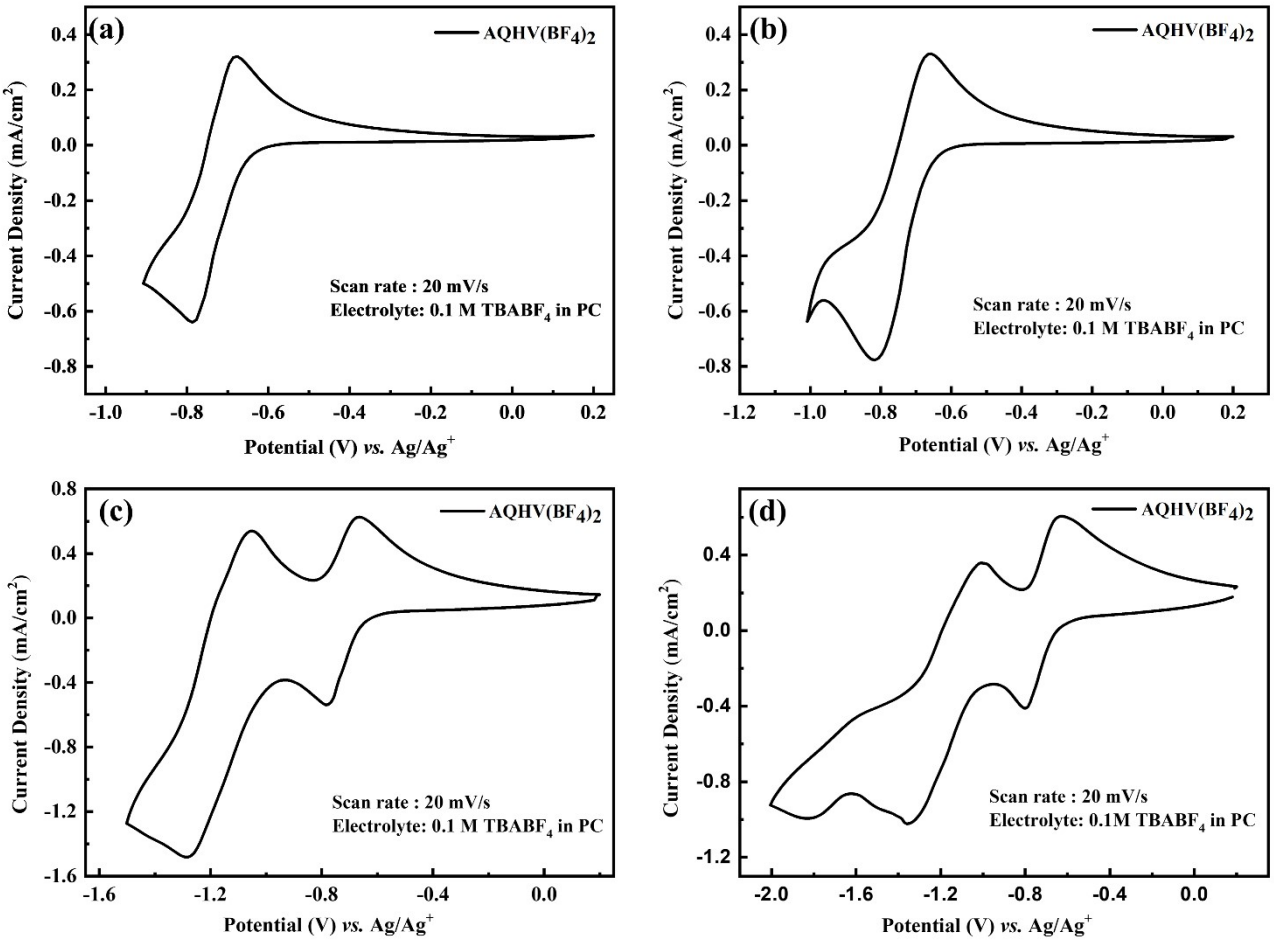

Figure S8. The cyclic voltammetry of AQHV(BF_4)$_2$ measured under different potential windows.

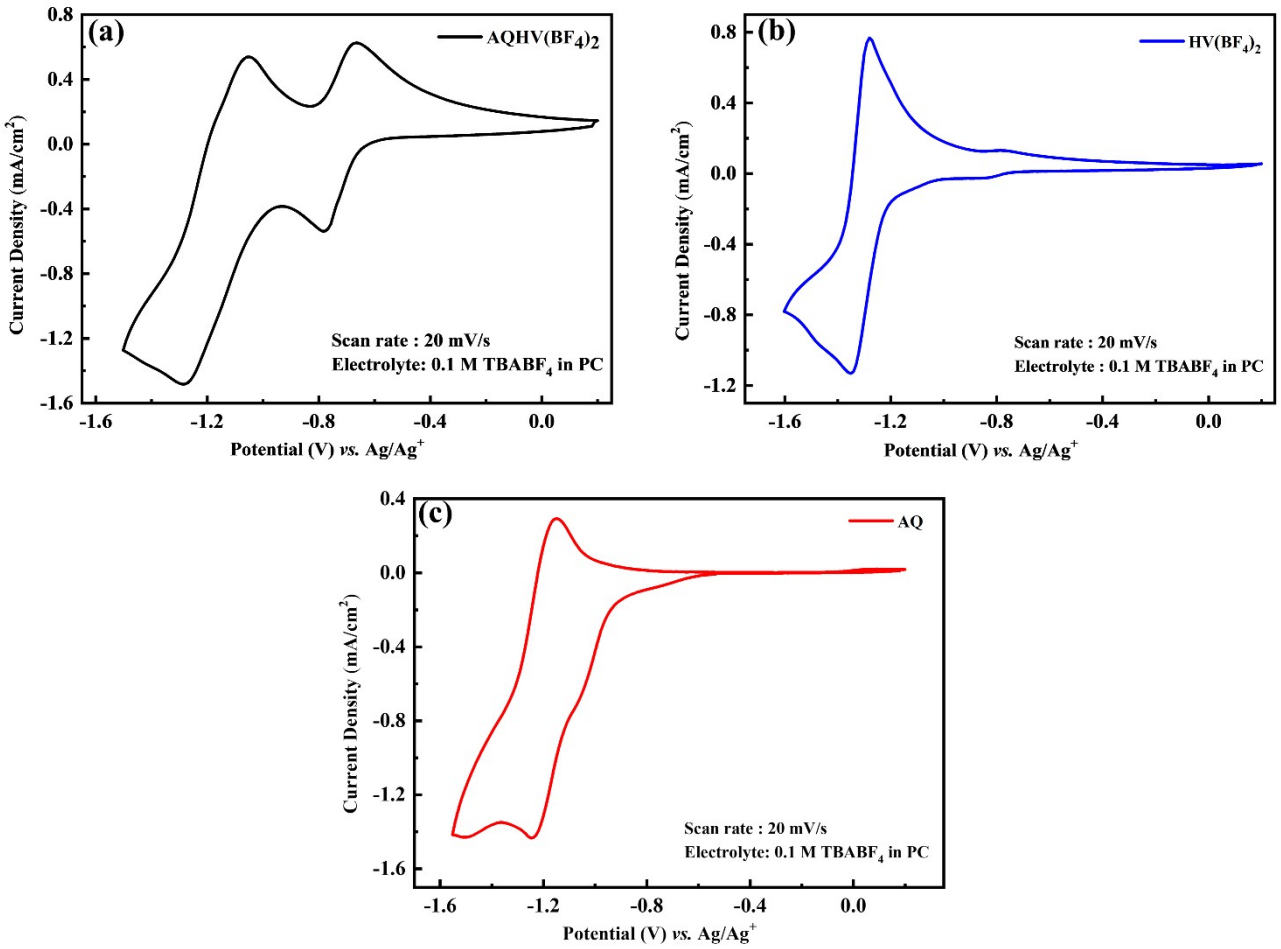

Figure S9. CVs of (a) $AQHV^{2+}$ (b) HV^{2+} and (c) 2-bromomethyl anthraquinone (AQ) respectively in $TBABF_4$/PC.

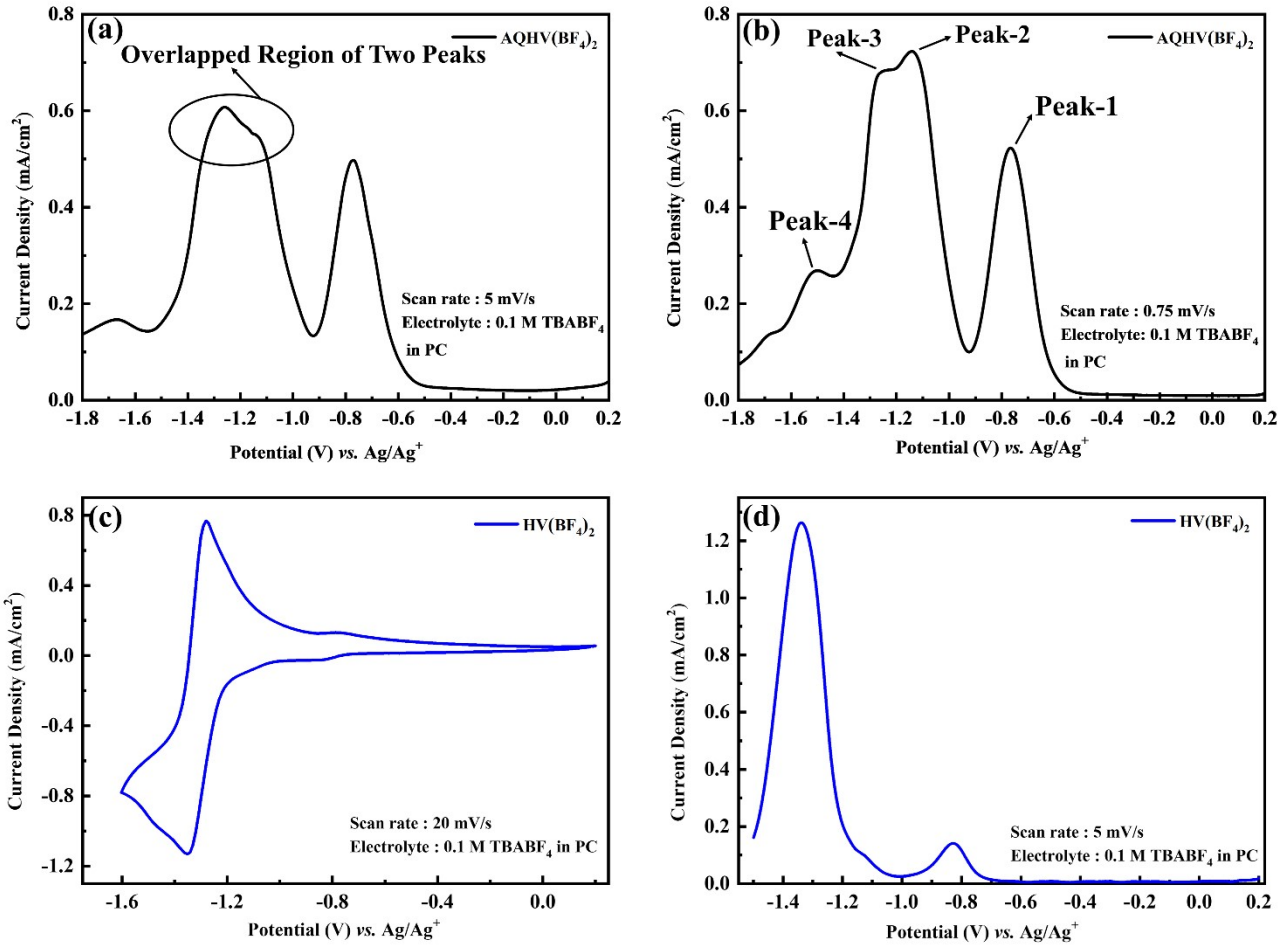

Figure S10. The cyclic voltammetry (CV) and differential pulse voltammetry (DPV) datas of (a) $AQHV(BF_4)_2$ and (b) $HV(BF_4)_2$ in $TBA(BF_4)$/PC respectively.

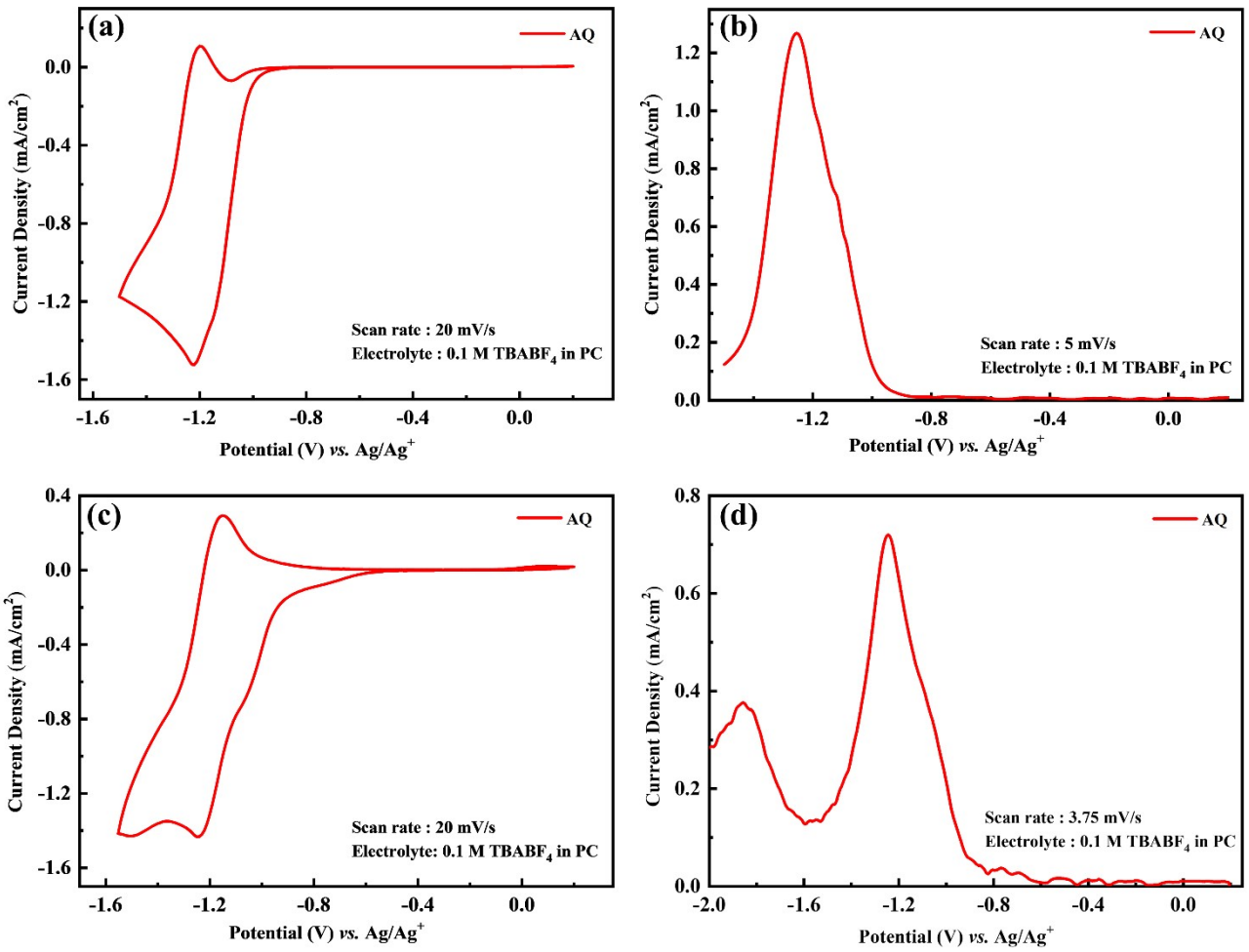

Figure S11. (a) The CV of (a) 2-bromomethyl anthraquinone (AQ) and (b) DPV of the AQ in the $TBA(BF_4)_2$ /PC in the potential window of -1.5 to +0.2 V, (c) the CV of AQ and (d) DPV of AQ in the $TBA(BF_4)_2$ /PC in the potential window of -2.0 to +0.2 V.

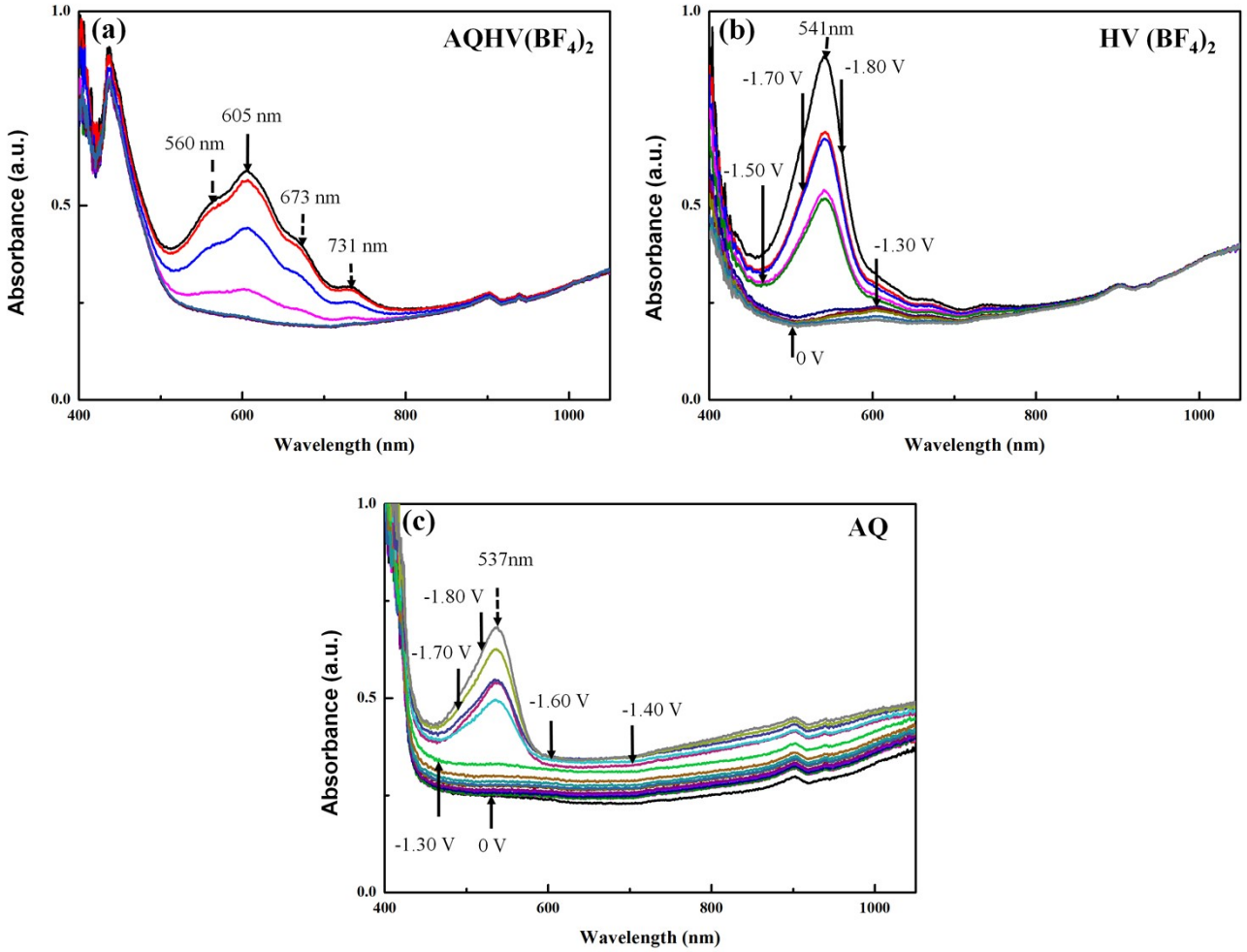

Figures S12. In-situ UV-Visible-NIR spectra of (a) 10 mM AQHV$(BF_4)_2$, (b) 10 mM HV$(BF_4)_2$ and (c) 10 mM 2-bromomethyl anthraquinone (AQ) species in TBABF4/PC solution.

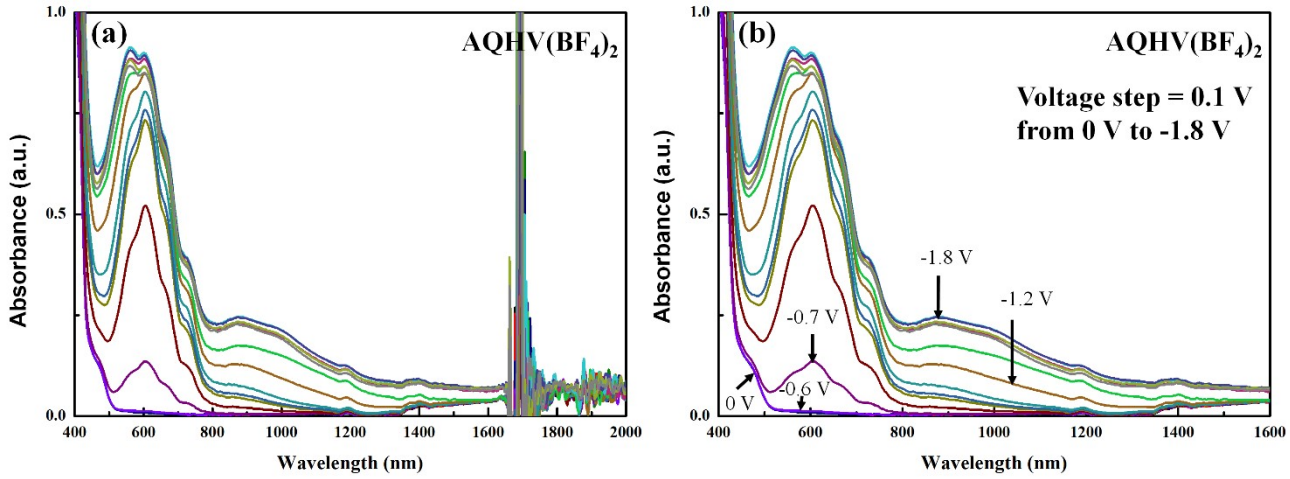

Figure S13. In-situ UV–Vis–NIR absorption spectra of AQHV(BF_4)$_2$ (10 mM) in 0.1 M TBABF_4/PC recorded during stepwise electrochemical reduction (a) in the range from 400 nm to 2000 nm and (b) zoomed-in region from 400 to 1600 nm.

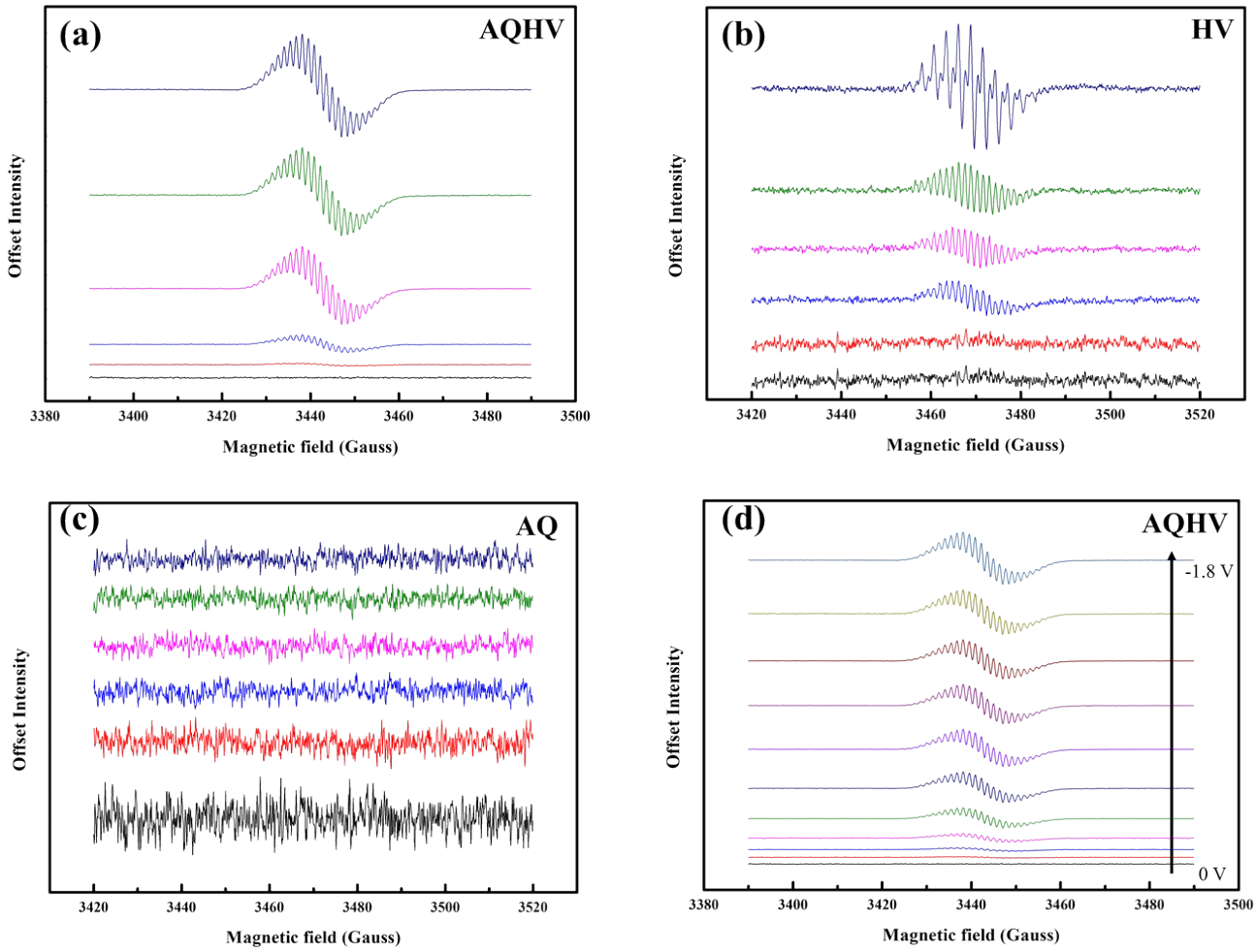

Figure S14. *In-situ* EPR spectra of (a) AQHV$(BF_4)_2$, (b) HV$(BF_4)_2$, (c) 2-bromomethyl anthraquinone (AQ) under stepwise electrochemical reduction conditions and (d) stepwise *in-situ* EPR spectra of AQHV$(BF_4)_2$ recorded at varying applied potentials (0.0 V to –1.8 V).

Table S1. Electrochromic performance-parameters of the s-ECD at the 1st cycle and 1000th cycle at two different wavelengths with an interval time of 10 s.

Cycle number	Potential (V)	λ (nm)	τ_b[a] (s)	τ_c[b] (s)	(T_b)[c] (%)	(T_c)[d] (%)	ΔT[e] (%)
1	0−1.2	605	2.5	2.1	75.7	15.5	60.2
1000	0−1.2	605	2.8	2.3	75.1	17.2	57.9
1	0−1.2	560	2.3	2.0	76.6	18.1	58.5
1000	0−1.2	560	2.5	2.2	76.1	19.7	56.4

[a]Bleaching time, [b]Coloring time, [c]Bleaching transmittance, [d]Coloring transmittance, [e]Transmittance change. Response time is defined as the time required to reach 95% of its saturated ΔT.

Table S2. Percentage of ΔT retained after 1000 and 4000 cycles of subjection of s-ECD and g-ECD at both the wavelengths. The potential window was between 0.0 and 1.5 V.

Type	Potential (V)	Wavelength (nm)	ΔT (%)	R^a_{1000} (%)	R_{4000} (%)
s-ECD	0−1.5	605	66.3	91.7	80.9
	0−1.5	560	65.6	92.4	81.0
g-ECD	0−1.5	605	67.5	93.0	63.4
	0−1.5	560	68.4	94.2	62.4

[a]R_n: Percentage of ΔT retained after n cycles.

Table S3. The values of g-factor obtained in the *in-situ* studies EPR studies of $AQHV^{2+}$.

Potential (V)	g-factor
−1.8	2.00369
−1.5	2.00369
−1.2	2.00369
−1.1	2.00370
−1.0	2.00370
−0.9	2.00370
−0.8	2.00370
−0.7	2.00372
−0.6	2.00375
−0.5	2.00356

References

1 R. D. Webster, R. A. W. Dryfe, J. C. Eklund, C.-W. Lee and R. G. Compton, *J. Electroanal. Chem.*, 1996, **402**, 167–174.

2 B. Gadgil, P. Damlin, E. Dmitrieva, T. Ääritalo and C. Kvarnström, *RSC Adv.*, 2015, **5**, 42242–42249.

3 M. Passon, A. Ruff, P. Schuler, B. Speiser and W. Leis, *J. Solid State Electrochem.*, 2015, **19**, 85–101.

4 M. Toybenshlak and R. Carmieli, *Isr. J. Chem.*, 2019, **59**, 1020–1026.